UNEC Journal of Engineering and Applied Sciences **SECTION:**
Vol. 6, No.1, 2026, pp. 108-114 **PHYSICS**
DOI: https://doi.org/10.61640/ujeas.2026.0510

Composition, structure and properties of WO_3 powders obtained by the arc discharge method

B.E. Umirzakov[1], K.B. Egamberdiyev[1], A.A. Abduvayitov[1], S.B. Donaev[1,2], J.B. Khujaniyozov[1], S.Z. Jafarova[3], D.A. Ibrahimova[3], R.G. Abaszade[1,2,4,5*]

[1]Tashkent State Technical University named after Islam Karimov, 2 University, Tashkent 100095, Uzbekistan
[2]Turan International Research Institute, 10A Aruz Mirzayev, Baku AZ1090, Azerbaijan
[3]Azerbaijan State University of Economics (UNEC), 6 Istiglaliyyat, Baku AZ1001, Azerbaijan
[4]Azerbaijan University of Architecture and Construction, 11 Ayna Sultanova, Baku AZ1073, Azerbaijan
[5]Azerbaijan State Oil and Industry University, 20 Azadliq, Baku AZ1010, Azerbaijan
email: *abaszada@gmail.com*

Abstract

The morphology, composition, and size of WO_3 nanoparticles were studied by using a scanning electron microscopy instrument (F200i(S)), an XPD-6100 X-ray diffractometer, and a NanoSight LM10 system before and after its immersion in an aqueous medium. The nanofluid was obtained by slowly and continuously stirring the water at a constant speed. The WO_3 nanoparticles were well dispersed in the aqueous medium and exhibited a relatively uniform size distribution. The results showed an average particle size of 176.1 ± 5.3 nm.

***Keywords*:** scanning electron microscopy, morphology, nanoparticles, arc discharge, laser beam, X-ray diffractometer, tungsten oxide, elemental analysis, nanoparticle trajectories.
PACS numbers: 61.66.Fn, 61.46.Hk, 81.05.Je

Received:	*Revised:*	*Accepted:*	*Published:*
30 January 2026	*5 March 2026*	*4 May 2026*	*31 May 2026*

1. Introduction

A great deal of attention is being paid to the production and study of the physicochemical properties of films and powders of W and tungsten oxides, which is associated with their widespread use in the creation of new types of catalysts, gas and chemical sensors [1-5], solar energy converters, multilayer MOS and SDS structures for UHF transistors, etc. at present time [6-9]. Many studies are devoted to the production of WO_3 electrodes for capacitors [10, 11], and the potential of composites based on tungsten oxide nanoparticles for the creation of supercapacitors is demonstrated.

The functional characteristics of tungsten oxides are largely determined by the features of their phase and chemical composition. In particular, tungsten trioxide is characterized by extensive polymorphism [12], which makes it possible to obtain materials with specified physicochemical properties, including a controlled band gap [13]. The presence of oxygen vacancies in the WO_3 structure determines the characteristics of its interaction with visible, UV, and near-IR radiation [14, 15], as well as the biological activity of materials based on it [16].

Many methods for synthesizing WO_3 have been developed, including solvothermal synthesis [17], chemical precipitation from solutions [18], electrochemical synthesis, physical

deposition from the gas phase [19], etc. up to now. One of the most convenient methods for producing tungsten trioxide is hydrothermal treatment, which ensures the production of materials with a given phase composition and morphology due to the possibility of varying the synthesis conditions over a wide range, including duration and temperature, composition of the reaction mixture, etc. [20].

In majority of cases, sputtering, ion implantation, and γ-laser irradiation are used to modify the properties of W and W oxides [21-24]. In recent years, crystalline phases and films with specified physical properties have been obtained on the surface layers of metals, semiconductors, and dielectrics using the low-energy ion implantation method, thanks to the possibility of controlled regulation of their energy band parameters [25-28].

It has been discovered that metals and their oxides are effective materials for use in nanofluids in recent years [29]. For example, Ni has already been used to create nanofluids in aqueous media. It is necessary to obtain metal and oxide nanoparticles and study their composition, structure, properties, and how these characteristics change when exposed to liquid to create nanofluids.

To fully understand the structural and property features of a "liquid-nanopowder" system, information about its initial components is essential. The physicochemical properties of nanoparticles depend greatly on their size and distribution in various liquids, requiring precise characterization methods. Nanoparticle trajectory analysis (NTA) is a powerful technique that allows particle size to be measured based on Brownian motion while simultaneously determining their concentration [30, 31].

The main aim of this research is to obtain nanosized particles (powders) of W and WO_3, to study their size, composition, structure and their changes during immersion in an aqueous medium.

2. Methods

WO_3 nanoparticles were obtained by the arc discharge method using a setup developed at the Institute of Ion-Plasma and Laser Technology [32]. The vacuum-arc setup is capable of implementing a stable process of vacuum-arc evaporation of tungsten with the introduction of a reactive gas, synthesizing tungsten oxide (WO_x) vapor. The vacuum chamber is made of stainless steel and is a cylindrical container with a diameter of 420 mm and a height of 400 mm. The required working vacuum in the process zone for vacuum-arc evaporation of tungsten is 0.1-0.01 Pa. A controlled amount of oxygen (O_2) is introduced into the chamber when obtaining tungsten oxide (WO_x). A highly pure tungsten rod with a diameter of 13 mm is used as a W source. The chamber is evacuated to a base pressure (~0.01 Pa) before the tungsten evaporation process begins. After reaching the base pressure, oxygen is introduced into the chamber through an adjustable inlet valve until the required operating pressure (~0.4 Pa) is established in order to obtain WO_3. The temperature in the WO_3 formation region is 2200 °C in this case [32].

The size, composition and structure of WO_3 nanoparticles were studied by using a scanning electron microscope (SEM) of the F200i(S) type and an XPD-6100 X-ray diffraction pattern.

Particle size distributions of WO_3 in an aqueous medium were measured by means of a NanoSight LM10 instrument (Malvern, UK) equipped with a sample chamber with a 405 nm and 642 nm laser with a built-in thermostat that ensures temperature stability in the range of 5-50 °C, and a syringe pump [33]. The syringe pump provides slow movement (flow) of liquid at a constant flow rate in the observation chamber. The movement of liquid at a constant flow rate leads to Brownian motion of the nanoparticles and is automatically controlled using NTA nanoparticle trajectory analysis software on a computer. A syringe pump can be used with syringes made of other materials, for instance, glass, but it is recommended to use only 1 ml plastic syringes in order to ensure a constant flow rate [34]. A

syringe pump reduces the photobleaching effect of fluorescent nanoparticles illuminated by a laser beam under resting conditions. Flow of fluorescent particles (or a probe) along the laser beam reduces the illumination time of each particle in the liquid. Non-photobleaching of nanoparticles in the field of view is constantly ensured by the instrument's filters in the observation and measurement areas, providing improved statistics.

A laser beam passes through the chamber and particles in the liquids situated in the beam's path scatter the light so that they can be easily observed through a 20-power magnification microscope on which the camera is mounted (figure 1). The laser module illuminates the particles with a specially aligned and focused laser beam. This allows very small particles (up to 10 nm) to be directly and individually visible using the microscope.

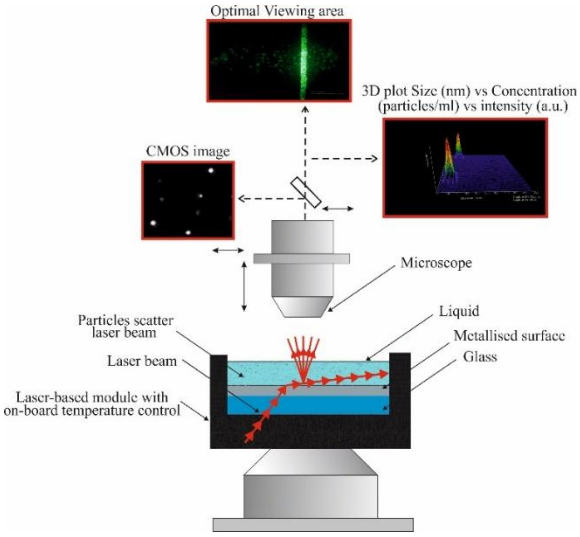

Figure 1. Schematic diagram of the NanoSight LM10 system for nanoparticle trajectory analysis

3. Results and discussion

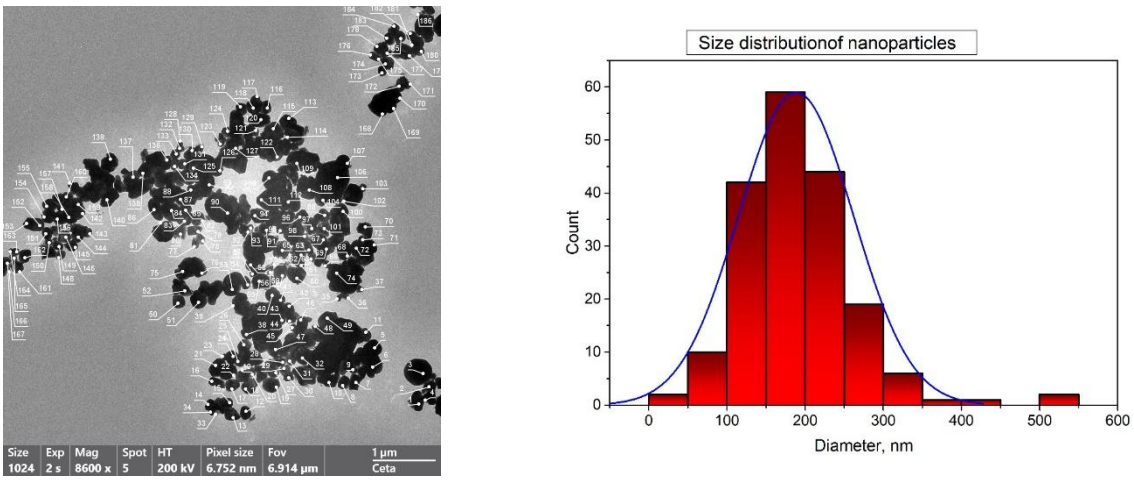

a) b)

Figure 2. SEM images of WO_3 particles: a) SEM images of the surface, b) Histogram of the size distribution of WO_3 nanoparticles

Figure 2a shows an SEM image of the surface of WO_3 nanoparticles, taken with the beam perpendicular to the surface. Both individual particles and agglomerates are visible in the figure. The particles have various shapes (spherical, tetrahedral, polygonal), but their average shape can be characterized as spherical. The average particle size ranges from 120 to

180 Å (figure 2b). The electron diffraction pattern of the WO_3 surface, shown in figure 3, allows to carry out an elemental analysis of the surface composition. In addition to intense tungsten and oxygen peaks, the electron diffraction pattern also contains peaks of the substrate (Cu) and carbon. The Cu and C peaks were ignored in the elemental composition calculations. Elemental analysis of the WO_3 nanoparticles shows that the oxygen concentration is ~76 at. %, and that of W is 24 at. %, which corresponds to the stoichiometric

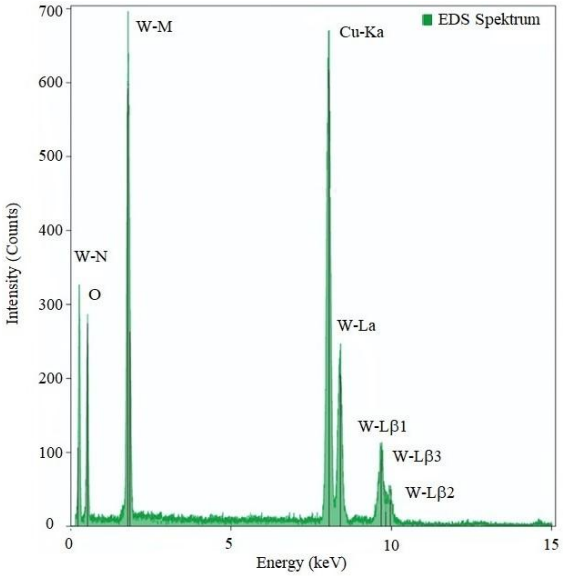

composition of WO_3 (table 1).

Figure 3. Elemental analysis of WO_3 nanoparticles applied to a copper substrate

Z	Element	Family	Atomic Fraction (%)	Atomic Error (%)	Mass Fraction (%)	Mass Error (%)
8	O	K	75,45	2,13	19,4	1,45
74	W	L	24,55	2,13	80,6	1,45

Table 1. Elemental analysis of WO_3 nanoparticles

Figure 4 shows the results of X-ray diffraction analysis of WO_3 nanoparticles. It follows from here that the phase and elemental composition are completely consistent with stoichiometric WO_3. The degree of crystallinity of the particles is ~30.52%. WO_3 has a monoclinic lattice with parameters a = 7.688 Å, b = 7.539 Å, and c = 10.515 Å.

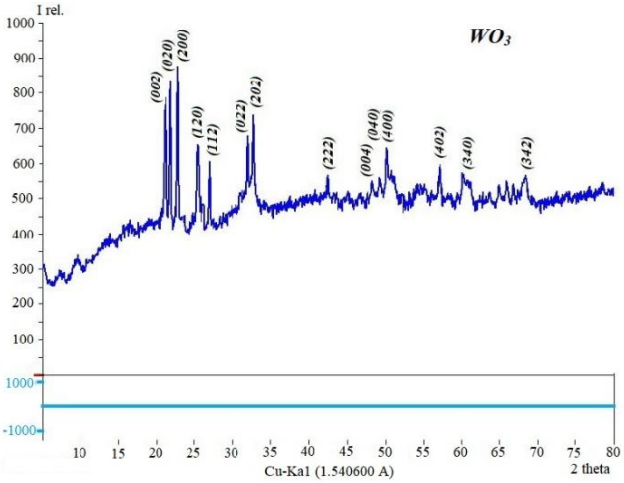

Figure 4. X-ray diffraction pattern of WO_3 nanopowders

Our further research focused on producing nanofluids using WO_3 powders. WO_3 powders were added to pure water, and the mixture was stirred using ultrasonic waves for this purpose. Figure 5 presents the results of an analysis of the size distribution of WO_3 nanoparticles in an aqueous media. The average nanoparticle size was 176.1 ± 5.3 nm with a standard deviation of 59.6 nm according to the measurement data. The nanoparticle concentration reached $7.39 \times 10^8 \pm 3.09 \times 10^7$ particles/mL. These parameters indicate a relatively high stability and uniformity of the dispersed system's size, demonstrating its potential for use in optoelectronic and photocatalytic applications.

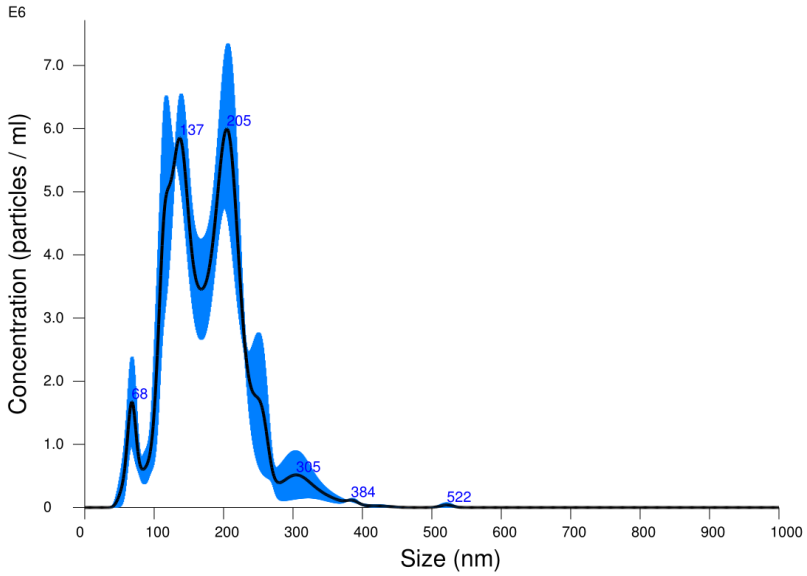

a)

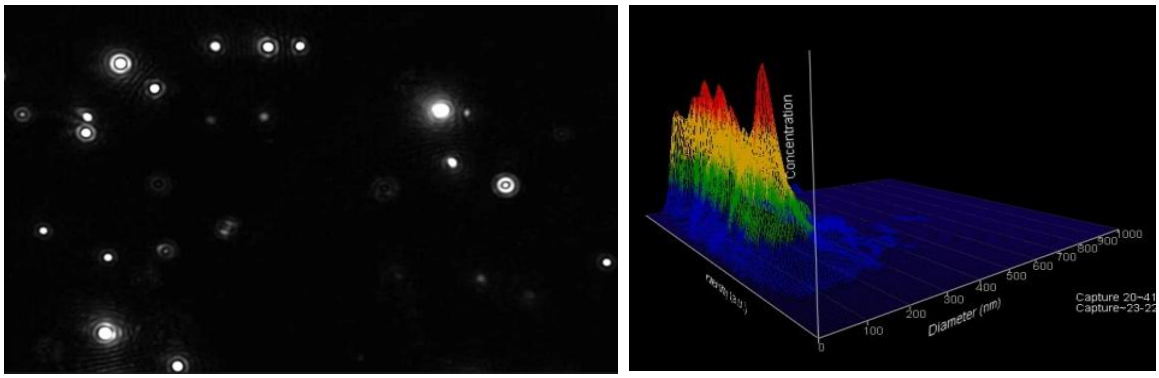

b)

Figure 5. a) Size distribution based on the results of measurements of nanoparticle tracking analysis of aqueous mixtures of WO_3 particles; b) with the corresponding video frame of nanoparticle tracking analysis and a 3D graph (particle size depending on intensity and concentration)

It should be noted that the nanoparticles were suspended in distilled water at room temperature (28.6–28.7°C) with a viscosity of 0.819–0.820 cP, typical for water under these conditions. Although specific dilution factors were not recorded, the analysis results revealed a narrow particle size distribution, with the vast majority falling in the 110–250 nm range. A plot of scattering intensity dependence on size confirmed the dominant contribution of particles in the 170–210 nm range, which is fully consistent with the modal size of the system. Analysis of the nanoparticle trajectories demonstrated that the WO_3 particles are well dispersed and characterized by a relatively uniform size distribution. The resulting average

size (approximately 176 nm) is optimal for processes in which the interaction of light with the nanoparticles and their high specific surface area plays a critical role. Such parameters are especially important for photocatalytic and optical applications, where increasing the surface area and active sites is directly related to process efficiency. Nanoparticle concentration values further confirm the stability of the resulting dispersion and its suitability for scaling in practical applications. Examples include application in gas sensors, electrochromic coatings, and photocatalytic reactors. Thus, it is clear that WO_3 nanoparticles have high potential for implementation in advanced technological solutions even at this stage. It should be noted that the observed polydispersity (SD ~60 nm) indicates the presence of partial aggregation or variations arising during the synthesis process. These factors can be eliminated or minimized by optimizing the synthesis conditions and using various stabilizing agents (e.g., surfactants or organic modifiers). A comparative analysis with literature data shows consistency between the obtained results and WO_3 nanoparticles synthesized by the arc discharge method, where the particle size range also varies from 100 to 250 nm. Thus, the experiments conducted confirm the potential of the synthesized WO_3 nanoparticles for applications in photocatalysis, sensorics, optoelectronics and energy. Further research is planned to establish the relationship between the size distribution of nanoparticles and their thermophysical properties, which will allow for targeted control of the characteristics of nanofluids for specific applied tasks.

4. Conclusion

The composition, size, and structure of WO_3 nanoparticles obtained by arc discharge followed by ball milling were studied by using SEM and X-ray diffractometry. The W concentration was found to be ~24-25 at. %, and θ ~75-76 at. %, with an average nanoparticle size of ~120-180 nm, the degree of crystallinity of nanoparticles is ~30.52%, and they have a monoclinic lattice. A nanofluid was obtained using ultrasonic displacement of WO_3 nanoparticles in water. Nanoparticle size distributions and trajectory analysis were determined by using a NanoSight LM10 instrument. It was found that the WO_3 nanoparticles were well dispersed in the aqueous media and exhibited a relatively uniform size distribution. The results showed an average particle size of particles is 176.1 ± 5.3 nm and a standard deviation of 59.6 nm. This research work was carried out with the financial support of a joint scientific project of the Ministry of Innovative Development of the Republic of Uzbekistan (project No. FL-8824063262) and the Belarusian Republican Foundation for Fundamental Research (grant No. T25UZB-013).

References

1. H. Zheng, J.Z. Ou, M.S. Strano, R.B. Kaner, A. Mitchell, and K. Kalantar-zadeh, Adv. Funct. Mater. **21**(12) (2011) 2175.
2. P.T. Moseley, Meas. Sci. Technol. **28(8)** (2017) 082001.
3. Yu.S. Gayduk, O.G. Reutskaya, A.A. Savitsky, and I.A. Taratin, Instruments and Methods of Measurements **7**(1) (2016) 41.
4. B. Urasinska-Wojcik, T.A. Vincent, M.F. Chowdhury, and J.W. Gardner, Sensors Actuators B **239** (2017) 1051.
5. Y. Alesanco, A. Vinuales, J. Rodriguez, and R. Tena-Zaera, Materials **11**(3) (2018) 414.
6. A.L.-S. Eh, A.W.M. Tan, X. Cheng, S. Magdassi, and P.S. Lee, Energy Technol. **6**(1) (2018) 33.
7. N. Cui, W. Li, Z. Guo, X. Xu, and H. Zhao, Catalysts **8**(6) (2018) 225.
8. P. Dong, G. Hou, X. Xi, R. Shao, and F. Dong, Environ. Sci.: Nano **4** (2017) 539.
9. C. Byrne, G. Subramanian, and S.C. Pillai, J. Environmental Chem. Eng. **6**(3) (2018) 3531.
10. Z. Hai, M.K. Akbari, Z. Wei, C. Xue, H. Xu, J. Hu, and S. Zhuiykov, Electrochim. Acta **246** (2017) 625.

11. M. Qiu, P. Sun, L. Shen, K. Wang, S. Song, X. Yu, S. Tan, C. Zhao, and W. Mai, J. Mater. Chem. A **4** (2016) 7266.
12. B. Han, A.L. Popov, T.O. Shekunova, et al., J. Nanomater. **2019** (2019) 5384132.
13. W. Smith, Z.-Y. Zhang, and Y.-P. Zhao, J. Vac. Sci. Technol. B Microelectron. Nanom. Struct. **25**(6) (2007) 1875.
14. Y. Xin, H. Zhou, X. Ni, et al., RSC Adv. **5**(71) (2015) 57757.
15. J. Yan, T. Wang, G. Wu, et al., Adv. Mater. **27**(9) (2015) 1580.
16. A.L. Popov, B. Han, A.M. Ermakov, et al., Mater. Sci. Eng. C **108** (2020) 110494.
17. Y. Fan, X. Xi, Y. Liu, et al., J. Phys. Chem. Solids **140** (2020) 109380.
18. D. Susanti, A.A.G.P. Diputra, L. Tananta, et al., Front. Chem. Sci. Eng. **8**(2) (2014) 179.
19. Z. Xia, H. Wang, Y. Su, et al., Coatings **10**(6) (2020) 577.
20. K. Ghosh, A. Roy, S. Tripathi, S. Ghule, A.K. Singh and N. Ravishankar, J. Mater. Chem. C **5**(29) (2017) 7307.
21. F. Can, X. Courtois, and D. Duprez, Catalysts **11**(6) (2021) 703.
22. V. Hariharan, V. Aroulmoji, C. Sekar, A. Shanthakumar et al., Int. J. Adv. Sci. Eng. **3**(299) (2016) 299.
23. T. Varga, H. Haspel, A. Kormányos, C. Janáky, Á. Kukovecz, Z. Kónya, Electrochim. Acta **256** (2017) 299.
24. C.M. Wu, S. Naseem, M.H. Chou, J.H. Wang, and Y.Q. Jian, Front. Mater. **6** (2019) 49.
25. A.A. Abduvayitov, G. Imanova, D.A. Tashmukhamedova, Kh.Kh. Boltaev, and B.E. Umirzakov, Scientific Herald of Uzhhorod University. Series “Physics” **54** (2023) 27.
26. B.E. Umirzakov, D.A. Tashmukhamedova, and K.K. Kurbanov, J. Surface Invest.: X-ray, Synchrotron Neutron Tech. **5**(4) (2011) 693.
27. S.B. Donaev, A.K. Tashatov, and B.E. Umirzakov, J. Surface Invest. **9**(2) (2015) 406.
28. Z.A. Isakhanov, Z.E. Mukhtarov, B.E. Umirzakov, and M.K. Ruzibaeva, Tech. Phys. 56(4) (2011) 546.
29. J. Schülein, I. Minrath, R. Pommersheim, and H. Löwe, J. Flow Chem. **4** (2014) 44.
30. V. Filipe, A. Hawe, and W. Jiskoot, Pharm. Res. **27**(5) (2010) 796.
31. U. Yokubov, K. Egamberdiev, B. Allaev, O. Trunilina, S. Telyaev, and M. Gafurova, J. Chem. Technol. Metall. **58**(5) (2023) 932.
32. I.K. Khudaykulov, J.R. Ravshanov, K.B. Ashurov, V.N. Arustamov, and D.T. Usmanov, J. Surface Invest.: X-ray, Synchrotron Neutron Tech. **16**(4) (2022) 599.
33. K. Egamberdiev, S.Z. Mirzaev, and U. Kaatze, J. Phys. Chem. B **120**(48) (2016) 12379.
34. B. Carr, P. Hole, A. Malloy, and P. Nelson, M. Wright, J. Smith, Nano Today **4**(5) (2009) 27.